*International Society for Rock Mechanics and Rock Engineering*
*Norwegian Group for Rock Mechanics*

*ISRM International Symposium*
*Eurock 2025 – Expanding the Underground Space*
*Trondheim, Norway, 16-20 June*
*ISBN 978-82-8208-079-8*

# Effect of Splay Branch on Fault Shear Reactivation and Micro-seismicity: A Discrete Element Analysis

Lie Kong[1, *], Milos Katchkin[2], Junlong Shang[1]
[1] *Department of Civil Engineering and Management, The University of Manchester, Oxford Road, Manchester, M13 9PL, UK*
[2] *Mott Macdonald, 319 St Vincent St, Glasgow, G2 5LD*
** lie.kong@manchester.ac.uk*

## Abstract

Underground infrastructures, such as tunnels, hydrocarbon reservoirs, and geothermal and $CO_2$ storage sites, are often influenced by faults that can compromise their integrity and reliability. Splay faults (also known as branch faults) are frequently observed along main faults, yet their impact on fault shear behaviour remains poorly understood. In this study, we employ the Discrete Element Method (DEM) to investigate how splay faults affect fault shear reactivation and the associated micro-seismicity. The fault is modelled as a damage zone, and we compare a planar fault with a splay fault angled at 30° to the main fault. In the numerical models, the main fault is positioned along the centreline. Shear reactivation is simulated by driving particles along one edge of the model, while monitoring shear stresses, cracking processes, and micro-seismic events across the different scenarios. The results demonstrate that the presence of a splay structure significantly influences stress distribution within the faults. In the planar fault model, stress evolves uniformly at first but later exhibits fluctuations due to fault reactivation. Fractures in this model remain confined within the fault zone. In contrast, the splay fault model shows earlier fault reactivation and more complex fracture patterns. These include prominent shear fractures near the intersections of the splay and main fault, extending into the surrounding host matrix. Micro-seismicity analysis reveals that both models predominantly produce small-to-moderate magnitude events. However, the splay fault model is characterized by larger maximum magnitudes, a wider range of event magnitudes, and a lower b-value. Regional segmentation of micro-seismicity in the splay fault model indicates frequent small events occurring along the splay branch, while the host matrix experiences fewer, but sporadically larger, seismic events.

## Keywords

Fault, shear, fracturing, discrete element method, micro-seismicity

# 1 Introduction

Fault systems, ranging from small to large scales, are common underground. These geological structures play a critical role in influencing the stability of subsurface infrastructures such as tunnels, hydrocarbon reservoirs, geothermal facilities, and $CO_2$ storage sites(Matsuki et al., 2010). Consequently, understanding the mechanical and seismic behaviours of faults under stress is fundamentally important for evaluating risks and ensuring the reliability of these systems. While planar faults have been extensively studied, secondary structures such as splay faults (i.e., branch faults that deviate from the main fault plane) remain less well understood. These structures, often observed in natural fault systems, significantly influence stress redistribution, rupture dynamics, and micro-seismic activity.

Fault systems are typically subjected to shear loads and exhibit stick-slip behaviour characterized by alternating periods of stress accumulation (stick) and abrupt displacement (slip) (Goebel et al., 2017; Rivière et al., 2018). The intermediate stage between stick and slip can be prolonged, during which fault zones may undergo cementation. Fault slip cycles can thus be considered reactivation processes, where stress is accumulated and then released through mechanical failure. Fault reactivation is a key process that governs the mechanical behaviour and seismic response of faulted rock masses.

Previous studies, including experimental investigations and numerical modelling, have predominantly focused on simplified fault geometries, such as planar faults or faults filled with weaker gouge materials (Bahaaddini et al., 2016; Goebel et al., 2017; Mair and Abe, 2011; Rivière et al., 2018; Zhao, 2013). While these studies have yielded valuable insights, they often do not fully capture the complexity of natural fault systems. Secondary structures like splay faults are expected to significantly modify stress fields, influence rupture propagation, and alter fracture development. Understanding the interplay between primary and secondary fault structures is therefore essential for advancing fault mechanics and assessing associated risks in both geological and engineering contexts.

To address this knowledge gap, this study employs the particle-based Discrete Element Method (DEM) to investigate the influence of splay faults on fault shear behaviour and associated micro-seismicity. Simplified numerical models are constructed to represent faults with and without splay structures. Direct shear is simulated along the main fault plane, and the resulting stress distributions, cracking processes, and seismic events are analysed.

The findings from this study aim to enhance the understanding of fault mechanics, particularly the effects of fault geometry on stress redistribution and rupture dynamics. This improved understanding is crucial for the design and safety assessment of subsurface infrastructures situated in faulted rock masses.

# 2 Numerical methodology

## 2.1 Discrete Element Method

The particle-based Discrete Element Method (DEM) was employed in this study to investigate the problem. DEM, a numerical technique introduced in the 1970s, has been extensively applied to explore issues in rock mechanics (Kong et al., 2022; Kong and Shang, 2024; Shang et al., 2018]{Shang, 2018 #1477). For the simulations in this study, the commercial DEM software Particle Flow Code (PFC), developed by Itasca, was utilized.

In a DEM model, solid materials are represented as assemblies of discrete particles, which are interconnected through inter-particle bonds (commonly referred to as “contacts”). These contacts are governed by a constitutive law that specifies the relationship between inter-particle forces and relative displacements. When subjected to external loads, DEM particles can move relative to each other, thereby replicating the material’s deformation behaviour. The motion of these particles is determined using Newton's Second Law, described as,

$$F_i = m_i\left(\ddot{x}_i - g\right) \tag{1}$$

where $F_i$ is the resultant force acting on a particle $i$; $m_i$ is the mass of particle $i$; and $\ddot{x}_i$ is the second-order derivative of displacement with respect to time, which represents acceleration; $g$ denotes the gravity acceleration.

$F_i$ regarding a particle is computed as the summation of all the contact force, in vector forms, on a particle, written as,

$$F_i = \sum_{j=1}^{n_c} f_j \tag{2}$$

where $f_j$ is the force on contact $j$; $n_c$ is the total counts of contacts on a particle; and Σ is a vector summation.

When the force at a contact exceeds its strength, the contact breaks, resulting in the formation of a crack. Each contact is characterized by a tensile strength and a shear strength. Depending on which strength threshold is exceeded at the point of rupture, the crack is classified as either a tensile crack or a shear crack.

The force-displacement law describes the contact force as a function of the relative displacement between two particles at a contact. This relationship is expressed as follows:

$$f_j^l = k_j^l u_j^l \tag{3}$$

where $k_j^l$ is the decomposed contact stiffness, with $l$ representing the normal ("n") and shear ("s") components, respectively; and $u_j^l$ is the displacement defined as the relative movement between the two contacting particles.

## 2.2 Numerical Models

Two numerical models are considered: one represents a planar fault, and the other represents a splay fault (Fig. 1). Both numerical models have dimensions of 7 cm in the x-direction and 4 cm in the y-direction. One model contains 27,744 DEM particles and 74,286 inter-particle contacts, which is considered to be sufficient to simulate deformation and cracking behaviour.

The planar fault model includes a single fault (i.e., the main fault) located at the centre of the model (see Fig. 1a). While the splay fault model includes both a main fault and a splay branch oriented at 30° to the main fault direction (see Fig. 1b). To account for the typical damage zone associated with faults, the fault is modelled as a narrow zone with reduced strength and modulus (the detailed micro mechanical parameters are provided in Section 2.3). Both the main fault and the splay branch have the same width of 3.0 mm, while the splay branch has a length of 15 mm.

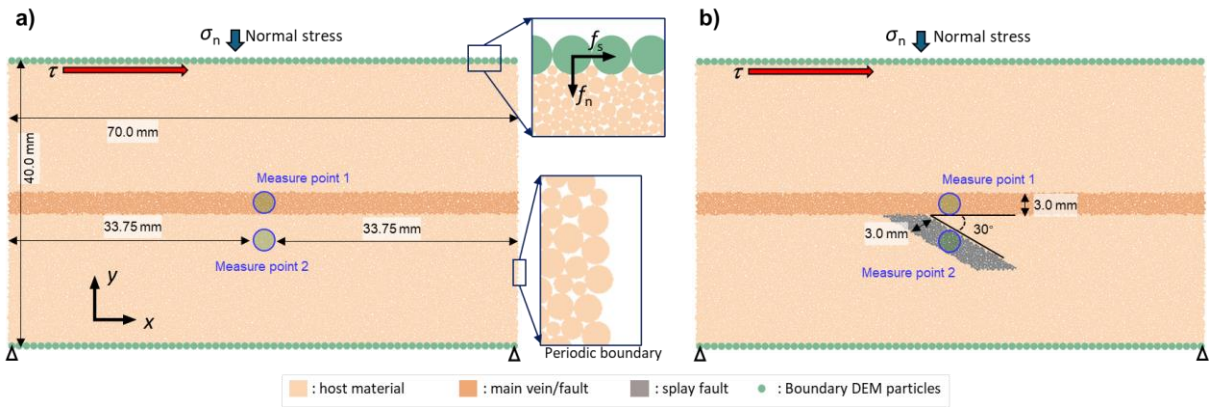


Fig. 1 Established numerical models for planar fault (a) and splay faults (b).

During simulation, the shear and normal forces are provided by the DEM particles (in green) on the top edge. The normal stress is kept consistent at 7.5 MPa. The lower boundaries of the two models are fixed. The left and right boundaries of the models are applied with a periodic boundary logic, with which the particles that move out of the right boundary will automatically entre the domain from the left side. The periodic boundary can simulate an infinite displacement. To monitor the evolution of

shear stress, two measure circles are placed at the centres of the main fault and splay fault, as seen in Fig. 1.

## 2.3 Micro-mechanical parameters

In the DEM model, certain constitutive contact models with certain mechanical properties (i.e., micro-mechanical parameters) are assigned to the particles and contacts to yield the mechanical properties of the simulated materials. Here we calibrate the mechanical properties of the host formation to basalt specimens from the Cornwall area in England, UK. The flat-joint constitutive contact model is used in this study, which has been demonstrated to have good capabilities in simulate hard rocks(Kong et al., 2021; Kong et al., 2024). Each flat-joint contact used here incorporates five segments that are capable of independently break. The average uniaxial compression strength of the specimens is 143.5 MPa and the mean elastic modulus is 36 GPa. As a fault is often associated with a damage zone, the fault zones in the models are considered by reduced strength and modulus. The contact tensile strength and cohesion are reduced to 30% of those of the host formation. The strength and cohesion of the contacts on the interfaces between the fault and host formation are 60% of those of the host formation. Table 1 lists the main micro mechanical parameters that are calibrated for the numerical models.

Table 1 Calibrated micro-mechanical parameters used in the numerical simulation

| **Micro-parameters** | **Host material** | **Fault** | **Fault interface** |
|---|---|---|---|
| Particle density, kg/m3 | 3300 | 3120 | - |
| Tensile strength, σ (MPa) | 31.0 | 9.6 | 18.6 |
| Cohesion, C (MPa) | 55.0 | 16.5 | 33.0 |
| Contact effective modulus, $E_{eff}$ (GPa) | 50.0 | 30.0 | - |
| Normal-to-shear stiffness ratio, s (-) | 2.4 | 2.4 | - |
| Bond friction coefficient, μ (-) | 0.25 | 0.1 | 0.18 |
| Friction angle, ϕ (°) | 48.0 | 50 | 49 |
| Number of elements in each flat-joint contact, $n_r$ (-) | 5 | 5 | 5 |

## 2.4 Simulation of micro-seismic events

The simulation of micro-seismic (MS) events in this study is based on the approach introduced by Hazzard and Young (2004), which models the phenomenon as the rupture of inter-particle contacts. In the algorithm, contact ruptures that occur in close spatial and temporal proximity are grouped as part of the same micro-seismic event. Consequently, a single MS event may involve one or multiple cracks.

When a contact ruptures, the forces acting on nearby contacts are redistributed. These changes in forces are used to calculate the moment tensor of the MS event, as expressed below,

$$m_{i,j} = \sum_{S} \Delta F_i R_j \tag{4}$$

where, $m_{ij}$ represents an element of the MS moment tensor, $\Delta F_i$ denotes the change in the contact force at a crack-enclosing contact, and $R_j$ is the distance between the contact and the centroid of the MS event. $S$ refers to the enclosing surface surrounding the MS event.

Subsequently, the scalar moment of the MS event is calculated as per the expression provided by Silver and Jordan (1982), written as,

$$M_0 = \sqrt{\frac{\sum_{i=1}^{n} m_i^2}{2}} \tag{5}$$

where, $m_i$ is the $i$-th eigenvalue of the moment tensor matrix; $n$ is the dimension of the model.

Based on the scalar moment, the moment magnitude ($M_w$) is further obtained by (Scholz, 2019),

$$M_w = \frac{2}{3}\log M_0 - 6 \tag{6}$$

Suppose the MS events follow a Gutenberg–Richter law (Gutenberg and Richter, 1944), then we have,

$$\log N = a - bW \tag{7}$$

where $N$ represents the number of events with magnitudes exceeding $W$. The constants $a$ and $b$ are parameters, where $b$ is commonly referred to as the $b$-value.

# 3 Results

In the simulation, we monitored the shear stress, fracturing behaviours, and micro-seismicity during the shear reactivation and investigate the influence of splay fault on the results.

Fig. 1 illustrates the evolution of shear stresses in the planar fault and splay fault models that are monitored at two measurement points during shearing. For the planar fault model, the shear stresses at both measurement points (Measure 1 and Measure 2) increase approximately linearly during the early stages, indicating uniform stress accumulation. In a later stage, the stresses exhibit fluctuations, indicating re-activations of the faults. In the splay fault model, the shear stresses at two measures also show a similar initial linear trend but diverges notably earlier suggesting advanced fault re-activation. The shear stresses at measure points 2 in two models are smaller than those measured at points 1, suggesting smaller shearing stresses off the central line. The shear stress in the splay fault branch was increased from a negative at the beginning point, which implying a stress reversion under a shearing load. The differences in the shear stress in the two models show that the emphasize the important role of secondary structures (e.g., splay branches) in stress redistribution and shearing dynamics.

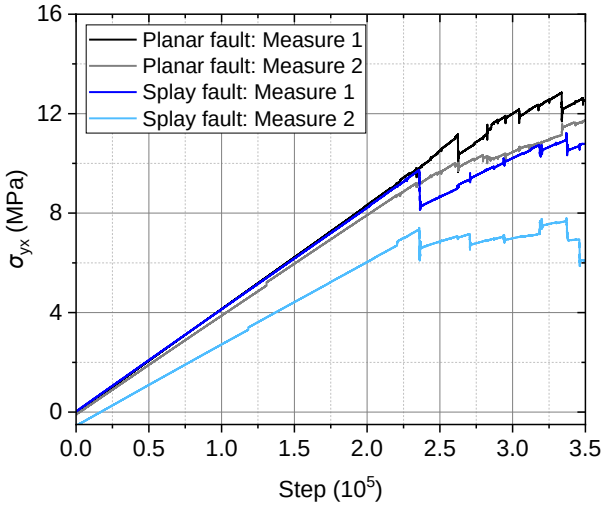


Fig. 2 Developments of shear stresses at the measure points in the two models

Fig. 3 shows the spatial and temporal development of fractures (both tensile and shear) during fault re-activation, as simulated in two numerical models. In each model, fractures are colour-coded, with tensile fractures represented in blue and shear fractures in green. In the planar fault model (top row), fracture development begins with the nucleation of tensile fractures along the fault plane. Both shear and tensile fractures are created. Over time, these fractures become more continuous and aligned with the fault orientation. No fractures are produced in the host matrix. The distribution of fractures suggests that the planar geometry does not promote significant shear failure away from the main fault. Instead, stress and fracture development are largely confined to the fault plane, with minimal off-fault damage. While in the splay fault model (bottom row), fracture evolution is more complex in the splay fault model due to the additional splay fault geometry. Initially, tensile fractures form along both the main fault and the splay branch. As re-activation progresses, shear fractures emerge and become more prominent along the splay branch, particularly near its intersection with the main fault. This reflects the localized intensification of shear stress caused by fault interactions. It appears that a segment of main fault right next to the splay branch sees a lower density of fractures, which may result from a stress shadow. The finial stage sees the formation of fractures in the host matrix that extend from the tips of the splay fault.

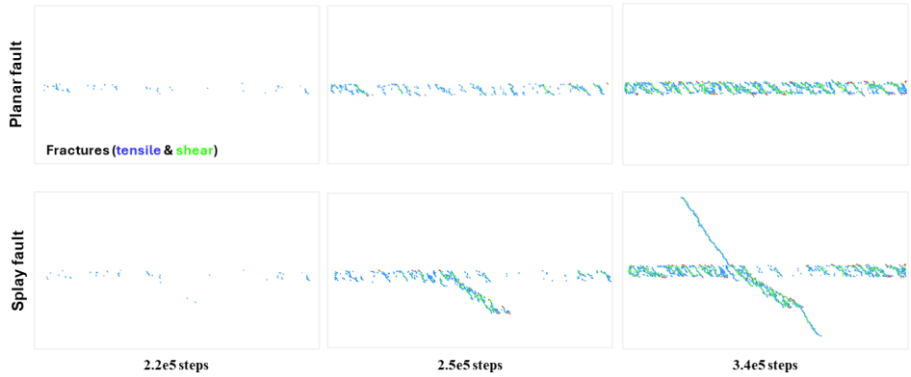


Fig. 3 Developments of fractures in the two models

Fig. 4 depicts the Gutenberg–Richter (G–R) relationship of micro-seismic (MS) events simulated during fault re-activation in two models. The histogram represents the frequency of MS events versus their magnitude, while the cumulative frequency-magnitude distribution (logarithmic scale) is shown as a line curve. Both models exhibit a characteristic distribution of micro-seismic magnitudes, with most events clustering around intermediate magnitudes. This indicates that small-to-moderate ruptures dominate fault re-activation, consistent with natural seismicity patterns. The planar fault model shows a narrower magnitude range, suggesting more uniform rupture processes. In contrast, the splay fault model produces a wider range of magnitudes, likely due to the complexity introduced by the secondary splay fault. The planar fault model shows a narrower magnitude range, suggesting more uniform rupture processes. In contrast, the splay fault model produces a wider range of magnitudes, likely due to the complexity introduced by the secondary splay fault. As seen, the splay fault produces larger maximum magnitudes. The slope of the linear portion, i.e., b-value, is a key parameter charactering the MS behaviour. A lower b-value is observed for the splay fault model.

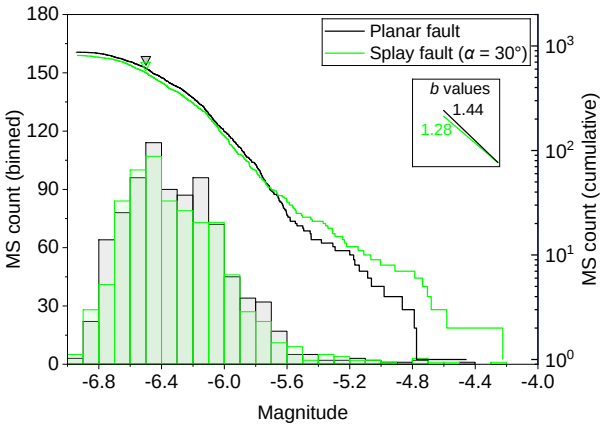


Fig. 4 Histogram of magnitudes and Gutenberg–Richter relation of micro-seismic events in the two models

Fig. 5 further illustrates the G–R relationship for MS events occurring within distinct regions of the splay fault model during fault re-activation. These regions include the main fault, the splay branch, the matrix, and mixed events (those spanning multiple regions). The results are segmented to analyse the seismicity characteristics across these zones. From Fig. 5, MS events within the main fault exhibit fewer large-magnitude events compared to smaller ones. This observation indicates consistent rupture behaviour and a relatively homogeneous stress distribution along the main fault plane. The splay fault branch shows a slightly higher b-value of 1.87 compared to 1.44 for the main fault. This suggests that smaller events dominate the splay fault branch, reflecting its enhanced capacity for accommodating distributed stress. In contrast, MS events in the matrix region are characterized by a lower overall frequency and limited large-magnitude events. The shallower slope (lower b-value) implies greater variability in stress concentrations and rupture dynamics in the matrix, resulting in fewer but more sporadic large-magnitude events.

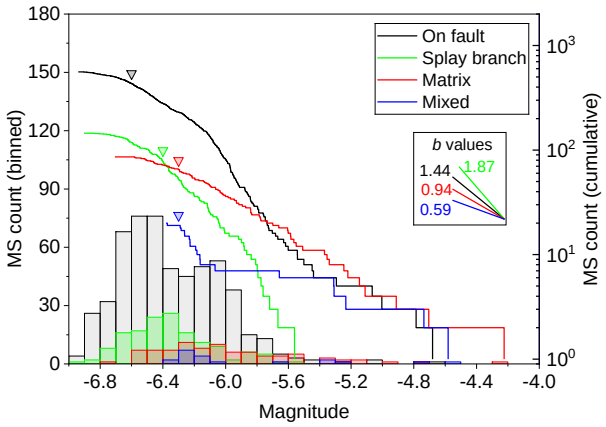


Fig. 5 Histogram of magnitudes and Gutenberg–Richter relation of micro-seismic events in different ranges in the splay fault model

# 4 Conclusions

This study investigates fault re-activation in planar and splay fault systems through analyses of shear stress evolution, fracture development, and micro-seismicity using DEM simulation. The planar fault model shows uniform stress evolution initially, followed by fluctuations due to fault re-activation, with fractures confined to the fault plane. In contrast, the splay fault model exhibits earlier fault re-activation and more complex fracture patterns, including prominent shear fractures near intersections and extending into the host matrix, reflecting localized stress intensification.

Micro-seismicity analysis reveals predominantly small-to-moderate magnitude events in both models, but the splay fault produces larger maximum magnitudes, a broader range of events, and a lower b-value, indicating heterogeneous stress and rupture dynamics. Regional segmentation in the splay fault model shows that the splay branch accommodates distributed stress through frequent small events, while the matrix experiences fewer but sporadic larger events.

These findings highlight the critical role of fault geometry and secondary structures in stress redistribution, rupture processes, and seismicity patterns, advancing our understanding of fault mechanics and associated seismic hazards.

# References

Bahaaddini, M., Hagan, P.C., Mitra, R., Khosravi, M.H., 2016. Experimental and numerical study of asperity degradation in the direct shear test. Engineering Geology 204, 41-52.

Goebel, T.H., Kwiatek, G., Becker, T.W., Brodsky, E.E., Dresen, G., 2017. What allows seismic events to grow big?: Insights from b-value and fault roughness analysis in laboratory stick-slip experiments. Geology 45, 815-818.

Gutenberg, B., Richter, C.F., 1944. Frequency of earthquakes in California. Bulletin of the Seismological society of America 34, 185-188.

Hazzard, J., Young, R.P., 2004. Dynamic modelling of induced seismicity. International journal of rock mechanics and mining sciences 41, 1365-1376.

Kong, L., Ranjith, P.G., Li, B.Q., 2021. Fluid-driven micro-cracking behaviour of crystalline rock using a coupled hydro-grain-based discrete element method. International Journal of Rock Mechanics and Mining Sciences 144, 104766.

Kong, L., Ranjith, P.G., Li, Q.B., Song, Y., 2022. Rock grain-scale mechanical properties influencing hydraulic fracturing using Hydro-GBM approach. Engineering Fracture Mechanics 262, 108227.

Kong, L., Shang, J., 2024. Cracking behaviour of mineralised fractures under direct-shear, ARMA US Rock Mechanics/Geomechanics Symposium. ARMA, p. D032S038R016.

Kong, L., Shang, J., Gamage, R.P., Li, B.Q., Song, Y., Cai, W., Ling, F., 2024. Grain-based DEM modelling of mechanical and coupled hydro-mechanical behaviour of crystalline rocks. Engineering Geology, 107649.

Mair, K., Abe, S., 2011. Breaking Up: Comminution Mechanisms in Sheared Simulated Fault Gouge. Pure and Applied Geophysics 168, 2277-2288.

Matsuki, K., Kimura, Y., Sakaguchi, K., Kizaki, A., Giwelli, A.A., 2010. Effect of shear displacement on the hydraulic conductivity of a fracture. International Journal of Rock Mechanics and Mining Sciences 47, 436-449.

Rivière, J., Lv, Z., Johnson, P., Marone, C., 2018. Evolution of b-value during the seismic cycle: Insights from laboratory experiments on simulated faults. Earth and Planetary Science Letters 482, 407-413.

Scholz, C.H., 2019. The mechanics of earthquakes and faulting. Cambridge university press.

Shang, J., Zhao, Z., Hu, J., Handley, K., 2018. 3D particle-based DEM investigation into the shear behaviour of incipient rock joints with various geometries of rock bridges. Rock Mechanics and Rock Engineering 51, 3563-3584.

Silver, P.G., Jordan, T.H., 1982. Optimal estimation of scalar seismic moment. Geophysical Journal International 70, 755-787.

Zhao, Z., 2013. Gouge Particle Evolution in a Rock Fracture Undergoing Shear: a Microscopic DEM Study. Rock Mechanics and Rock Engineering 46, 1461-1479.